First-order phase transitions by first-principles free-energy calculations: The melting of Al

Gilles A. de Wijs,* Georg Kresse,† and Michael J. Gillan
Physics Department, Keele University, Keele, Staffordshire, ST5 5BG, United Kingdom
(Received 9 September 1997)

The melting properties of aluminum are calculated from first-principles molecular-dynamics simulations using density-functional theory in the local-density approximation. We calculate a melting temperature of 890 K at zero pressure, to be compared to the experimental value of 933 K. An elaborate discussion of the techniques employed is presented. The solid- and liquid-state free energies are obtained *via* coupling constant integration. The respective reference systems are the quasiharmonic crystal and the Lennard-Jones fluid. Good quality of the Brillouin zone sampling is shown to be crucial. The strategy followed is expected to be applicable to a wide range of liquid metals. [S0163-1829(98)02914-2]

I. INTRODUCTION

Over the past two decades density-functional theory[1] (DFT) has developed into a very accurate technique for first-principles total-energy calculations. It has been extended to the description of dynamical processes on the atomic scale by Car and Parrinello,[2] and first-principles molecular-dynamics calculations and structural energy minimizations are now routinely performed by many groups. DFT has been very successful in the calculation of zero-temperature phase stability, i.e., total energies, and recently various applications involving free-energy calculations have been reported.[3–6] However, its application to first-principles finite-temperature phase stability calculation has remained limited to the study of Sugino and Car on the melting of silicon.[3]

In this paper we report on the determination of the melting point and other melting properties of Al, from first-principles calculations, using the full Kohn-Sham formalism throughout. We hope to demonstrate that DFT is capable of giving free energies with sufficient accuracy, and propose to apply the same technique to more challenging liquid metals in the future.

The main problem in a calculation on melting is the very high precision with which the free energy needs to be calculated. This need for high accuracy transpires from simple considerations: The entropy s, Gibbs free energy G, and temperature T are related by $-s=(\partial G/\partial T)_P$ (where P denotes the pressure). Therefore at melting the change with temperature of the difference between the solid-state and liquid-state free energies (ΔG) can be calculated from the entropy of fusion s_{m} via

$$s_{\mathrm{m}}=s_{\mathrm{liq}}-s_{\mathrm{sol}}=\frac{\partial G_{\mathrm{sol}}}{\partial T}-\frac{\partial G_{\mathrm{liq}}}{\partial T}=\frac{\partial \Delta G}{\partial T}. \tag{1}$$

It follows that δG, i.e., the maximum error in ΔG, is constrained by the required accuracy of the melting temperature δT_{m} through: $\delta T_{\mathrm{m}}\approx \delta G/s_{\mathrm{m}}$. For Al, s_m is 1.38 k_{B},[7] so that for a $\delta T_{\mathrm{m}}<50$ K a $\delta G<0.006$ eV/atom is required. Such an accuracy puts very stringent demands on the convergence of the calculations. For liquid metals, in particular, the convergence with respect to **k** points is very demanding. Moreover, this accuracy is definitely higher than that with which DFT approaches reality. Therefore good agreement with experiment can only be expected if a substantial cancellation of errors occurs, and therefore the validity of the approach can only be tested *a posteriori*.

Several calculations of the melting properties of liquid Al have been reported in the literature.[8–11] The approach of Moriarty, Young, and Ross is based on generalized pseudopotential theory (GPT).[8] The solid-state free energy is obtained in the quasiharmonic approximation and the liquid-state free energy by fluid variational theory. Here the liquid-state free energy is calculated from a reference system that is tuned to closely approach the free energy of the liquid system with the effective Al pair potential constructed from GPT. This procedure is variational in that it yields an upper bound to the free energy of the effective pair-potential system. Pélissier also employs a perturbational approach, but based on a local model pseudopotential for the electron-ion interaction.[9] To calculate the free energy, he uses a variational approach for both solid and liquid. In the solid state his calculation proceeds (again) *via* the phonon spectrum, but also includes some corrections for anharmonicity. For the liquid state optimized cluster theory is used. Mei and Davenport use an embedded atom approach.[10] Straub *et al.* fit volume-dependent pair potentials to first-principles data.[11] Their liquid-state free energy is obtained *via* molecular-dynamics simulation by thermodynamic integration. The solid-state free energy is calculated either from molecular-dynamics (MD) simulation and a model fit or from quasiharmonic lattice dynamics. They find a very good value for the melting transition (955 K) giving hope that an approach entirely based on DFT can accurately reproduce experimental melting data. Our approach is similar to various previous calculations in that we calculate the free energy of the solid (initially) in the quasiharmonic approximation. However, contrary to all previous calculations on the melting of Al, our corrections for anharmonicity in the solid state and our liquid-state free energy are obtained from thermodynamic integration using first-principles molecular-dynamics simulation. This means that an intermediate stage involving the construction of a model interatomic potential (by either a fitting procedure or perturbation theory) is bypassed and that the free energies are obtained directly from first principles. Therefore our approach is more generally applicable in principle.

This paper is organized as follows: In Sec. II the techniques used are described in detail. Results of the application to the melting of Al and a discussion of the errors can be found in Sec. III. Discussion and conclusions are presented in Sec. IV.

II. CALCULATION METHODOLOGY

A. General strategy

We aim to calculate the temperature T_m at which aluminum melts under the condition of constant, ambient, external pressure (i.e., $P=0$). Therefore we need to determine where the Gibbs free energy of the liquid, $G_{liq}(P=0,T)$, drops below that of the solid, $G_{sol}(P=0,T)$. We calculate both of these functions separately and obtain the melting point as the temperature where they cross. This also gives information about other melting properties like the entropy of fusion and the change of volume. Moreover, using this strategy, we avoid many troubles related to finite-size effects (like artificially high free-energy barriers and large hysteresis) that can easily occur in a direct simulation of any first-order phase transition. In particular, calculations on small systems, which our first-principles simulations necessarily are, are prone to suffer from such problems.

In any first-principles calculation one is confronted with the problem of calculating the free energy of a system having two very different sets of degrees of freedom: the ionic positions and the electronic wave functions. The ionic positions are described sufficiently accurately by classical mechanics whereas the electrons require a quantum-mechanical treatment. The usual way out of this problem is *via* the adiabatic approximation, which generally still holds at finite temperature: The electrons respond very fast (i.e., instantaneously) to the atomic motion. So their free energy does not depend on the ionic velocities and it can be calculated with as input their temperature T and the N atomic positions ($\mathbf{R}$) only. In density-functional theory this calculation is done by minimization of the Mermin functional (Sec. II A 1). The resulting electronic free energy $\widetilde{F}(\mathbf{R},T)$ acts as the classical potential-energy function $U(\mathbf{R},T)$ for the atomic degrees of freedom. Using well-established simulation techniques, this potential-energy function (into which T enters as a parameter) can then be used to calculate the Helmholtz (F) and Gibbs (G) free energies from the atomic dynamics only (Sec. II A 2). By virtue of the decoupling between atomic and electronic motion these equal the respective free energies of the complete system, i.e., for F the following holds:

$$F(V,T)=-k_B T\,\ln\left[\frac{1}{\Lambda^{3N}N!}\int_V \exp[-\beta\widetilde{F}(\mathbf{R},T)]d\mathbf{R}\right], \tag{2}$$

where $\beta=1/(k_B T)$, Λ is the thermal de Broglie wavelength and V denotes the volume. Note that the terminology is inherently confusing: In Eq. (2) the electronic free energy $\widetilde{F}$ and the (Helmholtz) free energy of the complete system F are two very distinct functions.[12]

1. Interatomic interaction via DFT: The Mermin functional

At finite temperature T the electronic free energy $\widetilde{F}(\mathbf{R},T)$ is obtained by minimizing the Mermin functional[13] in the Kohn-Sham formalism,

$$\widetilde{M}[\{\phi_n\},\{f_n\},\mathbf{R},T]=\sum_n [f_n\langle\phi_n|T_s|\phi_n\rangle-k_B T\widetilde{S}(f_n)] + E^H[\rho]+E^{xc}[\rho]+\int d^3\mathbf{r}V^{ion}(\mathbf{r})\rho(\mathbf{r}) + \gamma_{Ewald}(\mathbf{R}), \tag{3}$$

with respect to the orbitals $\{\phi_n\}$ and the partial occupancies $\{f_n\}$ under the constraints of orbital orthonormality and charge conservation.[14] (To simplify the notation we have dropped the **k**-point index.) T_s is the kinetic-energy operator, E^H the Hartree energy, E^{xc} the exchange-correlation energy functional, γ_{Ewald} the Madelung energy of the ions, and V^{ion} the ionic potential. The electronic entropy $\widetilde{S}(f)$ and charge density $\rho(\mathbf{r})$ are given by

$$\widetilde{S}(f)=-[f\ln f+(1-f)\ln(1-f)],$$

$$\rho(\mathbf{r})=\sum_n f_n|\phi_n(\mathbf{r})|^2, \tag{4}$$

respectively. Note that the Mermin formulation implies a Fermi distribution for the $\{f_n\}$ according to the eigenvalues of the $\{\phi_n\}$ in the associated Euler equation. It needs to be kept in mind that the resulting Fermi-surface smearing [measured by $k_B T$ in Eq. (3)] serves a twofold purpose. At first, there is its physical significance in describing the electronic sub-system at finite T. Secondly, as an additional advantage, it smoothes the discontinuous jump at the Fermi surface. This results in a faster convergence of $\widetilde{F}$ with respect to the density of the **k**-point mesh.[14]

Several approximations need to be made to calculate the Mermin functional. The most important one is the calculation of the exchange-correlation functional in the local-density approximation. Moreover, since it is not known for finite T, it is approximated by the zero-T functional of Ceperley and Alder[15] in the parameterization by Perdew and Zunger.[16]

Another approximation is the pseudopotential approximation: Only the valence electrons are explicitly treated and the interaction between valence electrons and the atomic core is replaced by a smooth potential that accurately mimics the scattering at the ''frozen'' core electrons and nucleus. We use an ultrasoft pseudopotential[17,18] with nonlinear core-corrections[19] applied. Details are reported in Sec. II D.

Since the function $\widetilde{F}$ acts as the potential for the ionic motion, the interatomic forces are calculated by its differentiation with respect to the atomic positions and are conveniently obtained from the Hellmann-Feynman theorem.[20–22] Using these forces, molecular-dynamics simulations can be performed by direct minimization of the Mermin functional at each time step. This is the approach we have followed. It allows to use a larger time step then conventional Car-Parrinello-type dynamics, but at each time step several electronic minimization steps are required to obtain the elec-

tronic ground state with sufficient accuracy. Overall we expect that this approach is equally efficient as a standard Car-Parrinello-type dynamics (see Sec. II D for details).

2. Thermodynamic integration

Given the interatomic potential $U(\mathbf{R},T)$ [i.e., $\widetilde{F}(\mathbf{R},T)$] we need to calculate the Gibbs free energy $G(P,T)$. For both the liquid and the solid, we achieve this by first calculating the Helmholtz free energy, $F(V,T)$, from which we obtain G by

$$G(P,T)=F(V,T)+PV, \quad P=-\left(\frac{\partial F}{\partial V}\right)_{N,T}. \tag{5}$$

At ''ambient'' pressure $PV=0$. However, we still need to calculate $P(V,T)$ to find the zero-pressure volume.

It is well known that F cannot be calculated from a MD simulation directly, since it cannot be expressed as an ensemble average.[23] However, well-documented techniques do exist to calculate the free energy of a system relative to that of another system (see, e.g., Ref. 23 for a thorough overview). Thus it is possible to calculate the free energy of a system by relating it to the known free energy of a simple reference system, e.g., the ideal gas or the Lennard-Jones (LJ) fluid.[24] In MD simulations this is conveniently done by thermodynamic integration using Kirkwood's coupling constant method. A range of hybrid systems is introduced in which the potential-energy function U switches from the reference system ($\lambda=0$, $U=U_{\mathrm{I}}$) to the system for which one wants to calculate F ($\lambda=1$, $U=U_{\mathrm{II}}$):

$$U(\lambda)=(1-\lambda)U_{\mathrm{I}}+\lambda U_{\mathrm{II}}. \tag{6}$$

The difference between the free energies of systems I and II is obtained by integration over the range of hybrid systems:

$$F(\lambda=1)-F(\lambda=0)=\int_0^1 d\lambda\left\langle\frac{\partial U(\lambda)}{\partial\lambda}\right\rangle_{\lambda}, \tag{7}$$

where the brackets denote the ensemble average for a system with potential-energy function $U(\lambda)$. For each λ a separate MD run needs to be performed. It is important to choose a reference system that behaves like the system of interest, so that the integral is well approximated by only a few (ideally one) MD runs. We use this technique to calculate the free energy of the liquid (using the Lennard-Jones fluid as a reference), and the anharmonic corrections to the solid-state free energy (using the quasiharmonic crystal as reference). In principle, it is also possible to obtain the integral of Eq. (7) from one MD run, where λ switches adiabatically (i.e., very slowly) from 0 to 1 during the simulation.[25] However, we prefer to carry out MD runs for fixed λ since it allows for a systematic improvement of the integral, without having to redo part of the calculation: If the integral is calculated with an extended Newton-Cotes formula (like Simpson's rule), higher accuracy can be achieved by just adding values of the integrand at intermediate points obtained from new simulations.

B. Free energy of the solid phase

1. Quasiharmonic approximation for the crystal free energy

In the quasiharmonic approximation the Helmholtz free energy is determined by the harmonic lattice vibrations, i.e., the phonons, at a volume V:[26]

$$F(V,T)=U_0(V,T)+\frac{1}{\Omega_{\mathrm{BZ}}}\times\sum_i\int_{\mathrm{BZ}}\left(\frac{\hbar\omega_{\mathbf{q},i}}{2}+k_BT\,\ln[1-e^{-\hbar\omega_{\mathbf{q},i}/k_BT}]\right)d\mathbf{q}. \tag{8}$$

The $\{\omega_{\mathbf{q},i}(V,T)\}$ are the phonon angular frequencies at wave vector $\mathbf{q}$ and polarization direction i for volume V (see Ref. 27). Ω_{BZ} denotes the volume of the Brillouin zone. The first term, $U_0(V,T)$, is the potential energy (i.e., $\widetilde{F}$) of the perfect crystal at volume V. Both the $\{\omega_{\mathbf{q},i}\}$ and U_0 implicitly depend on temperature *via* the temperature dependence of the Mermin functional. The second term in Eq. (8) arises from the zero-point vibrational motion, and the third from the thermally-induced occupancy of the various phonon modes.

Note that Eq. (8) assumes a quantum statistics for the phonons, whereas our calculation of the liquid-state free energy is fully classical. In the high-temperature limit, Eq. (8) can be expanded into[26]

$$F(V,T)=U_0(V,T)-\frac{k_BT}{\Omega_{\mathrm{BZ}}}\times\sum_i\int_{\mathrm{BZ}}\left(\ln\left[\frac{k_BT}{\hbar\omega_{\mathbf{q},i}}\right]-\frac{1}{24}\left[\frac{\hbar\omega_{\mathbf{q},i}}{k_BT}\right]^2+\cdots\right)d\mathbf{q}. \tag{9}$$

The first term in the sum on the right-hand side is the classical contribution. For consistency with the liquid-state calculations, we discard the higher terms in the expansion, i.e., the quantum corrections. At $\sim$1000 K these are typically $\sim$1 meV/atom for Al.

As input for Eq. (9) we need the phonon density of states (PDOS) and $U_0(V,T)$. The latter is easily calculated in a primitive fcc cell with a very high $\mathbf{k}$-point density. Since these are small calculations, V and T dependence can be fully accounted for. The PDOS is obtained by interpolation of the phonon frequencies calculated with the method of Ref. 28. Here one uses a supercell approach with typically several tens of atoms. One (or more, if needed) atom is slightly displaced and the resulting forces on all the atoms are calculated. From these the interatomic force constants matrix $\mathbf{D}_V$, and *via* its diagonalization the dynamical matrix, are obtained. This approach is only exact for those phonons having wave vectors commensurate with the periodically repeated supercell. Phonon frequencies at other $\mathbf{q}$ points can also be calculated, assuming that the extra force constants needed are 0. This approximation can be tested by carrying out calculations for various sizes of the system.

The procedure is repeated at various volumes, and the results are fitted to a polynomial. From this fit and Eq. (5) the Gibbs free energy is obtained. In principle, the whole volume ''scan'' should be repeated for the range of temperatures of

interest, since the $\{\omega_{\mathbf{q},i}\}$ depend on temperature. For Al this temperature dependence is negligible: we checked that it induces a change in G of merely ~ 0.15 meV/atom for a 100-K temperature change. Therefore our calculations of the $\{\omega_{\mathbf{q},i}\}$ were carried out for a fixed Fermi smearing, corresponding to a temperature of 800 K.

2. Corrections for anharmonicity

In order to obtain the full free energy of the crystal a correction that reflects the anharmonicity of the lattice vibrations needs to be added to the quasiharmonic results obtained in the previous subsection. This is done by a thermodynamic coupling constant integration. U_{II} is the complete interatomic potential-energy function calculated from first principles, and the reference potential-energy function U_{I} is the fully classical quasiharmonic potential energy function for the $3N-3$ phonon modes in the N atoms supercell:

$$U_{\mathrm{I}}=U_0(V)+\frac{1}{2}\sum_{\mathbf{R},\mathbf{R}'}\mathbf{u}(\mathbf{R})\mathbf{D}_V(\mathbf{R}-\mathbf{R}')\mathbf{u}(\mathbf{R}'). \quad (10)$$

The $\mathbf{u}(\mathbf{R})$ are the atomic displacements from the equilibrium positions $\mathbf{R}$ and $\mathbf{D}_V(\mathbf{R}-\mathbf{R}')$ is the atomic force constants matrix. For Al we use a 32-atom supercell, i.e., $N=32$.

An issue that needs care is the temperature control during the MD runs. Since the system is close to (or completely) harmonic, the modes will not strongly couple and equilibration between the modes will be very slow. For this reason the standard Nosé thermostat technique[29] cannot be used, unless each ''normal mode'' receives its own dedicated thermostat. Moreover, the standard Nosé scheme has trouble in generating a canonical sampling for a harmonic oscillator and would need to be replaced by a chain of Nosé-Hoover thermostats.[30] (See Ref. 4 for a thorough discussion.) Another way out of these problems that we have adopted is to use a thermostat of Andersen type:[31] Each atomic velocity component is redrawn randomly from a Gaussian distribution after a specified, average number of steps.

The approach outlined so far results in the correction to the Helmholtz free energy for one (V,T) point. To obtain it as a function of volume, we fit a polynomial to the results of the correction scheme carried out at various volumes. For the temperature dependence of the correction we assume a T^2 scaling. In fact, the scaling of the corrections with temperature is not evident *a priori*. In general a combination of T^2, T^{-2} terms and even a temperature-independent contribution is expected in the high-temperature limit.[26] Therefore the temperature scaling needs to be checked by additional calculations at a few other temperatures.

Alternatively one could have adopted the strategy followed in Ref. 32 where a series of molecular-dynamics simulations at several temperatures are carried out and the coefficients of an analytic representation of the anharmonic contribution to F are obtained from a fit to, e.g., the internal energy after its harmonic part $(3k_{\mathrm{B}}TN/2)$ has been subtracted out. This approach is probably more useful if the free energy needs to be accurately known over a large temperature interval, but here we are interested in the the free energy only around the melting point. Therefore we expect the approach we have used to be more efficient in terms of computer requirements.

3. Contributions due to vacancies

At any nonzero temperature, a crystal always contains thermally generated lattice defects. These defects will give a contribution to the free energy, which is not accounted for in the discussion so far. We give here a brief discussion of this defect contribution; our conclusion will be that it can be neglected.

In aluminum and most other metals, the dominant lattice defect in thermal equilibrium is the vacancy.[33,34] For a crystal containing N_{latt} lattice sites and a concentration c of vacancies (number of vacancies per lattice site), the vacancy contribution G_{v} to the Gibbs free energy of the crystal is

$$G_{\mathrm{v}}=N_{\mathrm{latt}}[cg_{\mathrm{v}}+k_{\mathrm{B}}T(c\ \ln c+(1-c)\ln(1-c))]. \quad (11)$$

Here g_{v} is the free energy of a single vacancy, i.e., the change of free energy of the whole system when an atom is removed from a specified perfect-lattice site and used to create a new lattice site, the whole process being performed at constant pressure and temperature; the final term in Eq. (11) is the configurational free energy of the vacancies. In full thermal equilibrium, the concentration c is determined by the condition that G_{v} be a minimum, which gives

$$c=1/[\exp(g_{\mathrm{v}}/k_{\mathrm{B}}T)+1]. \quad (12)$$

The equilibrium value of G_{v} is thus

$$G_{\mathrm{v}}=N_{\mathrm{latt}}k_{\mathrm{B}}T\ \ln(1-c). \quad (13)$$

In practice, $c\ll 1$, so that the vacancy contribution to the free energy per atom is accurately approximated by

$$G_{\mathrm{v}}/N_{\mathrm{latt}}\simeq -k_{\mathrm{B}}Tc. \quad (14)$$

To estimate this free energy, we need to know c, or equivalently g_{v}, at the melting point. There have been several attempts to determine c experimentally, e.g., by accurate measurement of the lattice parameter and the density of the crystal.[33] Such measurements indicate that in Al just below the melting point $c\simeq 10^{-3}$. Using this value for c, we estimate a vacancy contribution to the free energy per atom of 0.1 meV. From the relation $\delta T_{\mathrm{m}}=\delta G/s_{\mathrm{m}}$ mentioned in the Introduction, this very small free-energy contribution could change T_{m} by at most a few K, and we therefore ignore it.

C. Free energy of the liquid phase

In the liquid state we need another strategy to determine the free energies. Using Eq. (5), as for the crystalline phase, we need to calculate F as a function of both V and T. This could be done by carrying out, for every point on a (V,T) grid, a coupling constant integration from a system with known free energy to the full first-principles system. This is not exactly our approach.

We carry out two coupling constant integrations (Sec. II C 1), at two different reference volumes $(V_{0,a},V_{0,b})$ and one reference temperature (T_0), that are chosen to be close to the experimental melting point. As a reference system we use the Lennard-Jones fluid. From this we obtain the Helmholtz free energy at the chosen thermodynamic state points. From additional MD runs (at the same two state points) we

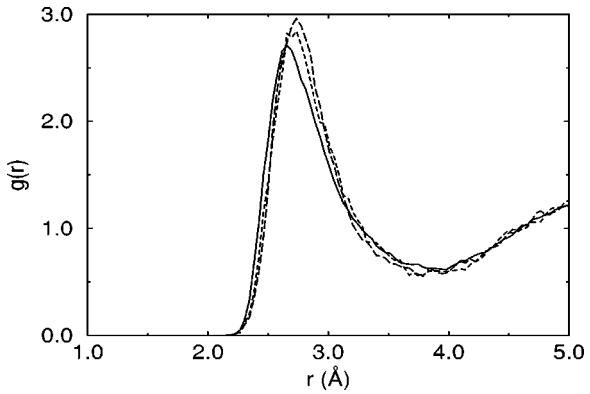

FIG. 1. LJ $g(r)$ (full curve), first-principles $g(r)$ from Γ point calculation (short dash), and first-principles $g(r)$ calculated with 4 **k** points (long dash). Averages pertain to 1.6 and 1.2 ps runs for the Γ and the 4 **k**-point calculations, respectively. $V=18.31$ Å^3/atom, $T=900$ K.

also obtain the internal energy E and pressure P. In principle, by thermodynamic integration along V and T, using

$$\left(\frac{\partial F}{\partial V}\right)_{N,T} = -P \quad \text{and} \quad \left(\frac{\partial F/T}{\partial 1/T}\right)_{V,N} = E, \tag{15}$$

it is possible to calculate $F(V,T)$ (and therefore G) in the vicinity of the chosen points. However, we find it more convenient to take a further intermediate step and fit the data to a simple model (Sec. II C 2). F, P, and G at nearby state points are obtained from the model.

1. Lennard-Jones reference system

For the two coupling constant integrations our reference system is the Lennard-Jones (LJ) liquid, which features the following pairwise additive interaction:

$$\phi(r)=4\epsilon\left[\left(\frac{\sigma}{r}\right)^{12}-\left(\frac{\sigma}{r}\right)^{6}\right], \tag{16}$$

where ϵ and σ are parameters.

Johnson *et al.* have carried out elaborate MD calculations on this system and have given an accurate tabulation and analytic fit for the Helmholtz free energy as a function of the reduced temperature $(T^*=k_BT/\epsilon)$ and density $[\rho^*=(N/V)\sigma^3]$.[24] This gives us the liberty to choose an optimal ϵ and σ. We tune them so that the LJ $g(r)$ closely fits the first principles $g(r)$. In doing so care has to be taken not to move the LJ system into the nonliquid region of its phase diagram. This is necessary to avoid the risk of the hybrid system undergoing a phase transition away from the liquid state during an MD run. In general, the LJ system can be made to fit the first-principles system very accurately (see Fig. 1 and Table I for details of the fits). Therefore, only very few runs are expected to be needed for the thermodynamic integration. Test calculations showed that the integral of Eq. (7) is already well approximated with the value of the integrand for the one run at $\lambda=0.5$ only (see Sec. III A 1 for details).

We comment that although the Lennard-Jones fluid provides a good reference system for liquid Al, it may not be the best reference system for other liquid metals. For example, for the d-bonded metals it has been argued that a potential of r^{-20} type should be more appropriate.[35,36] Even for liquid Al, LJ is not a unique choice, and a r^{-12} potential might work equally well.[35,36]

TABLE I. Details of the Lennard-Jones reference systems used for the coupling-constant integrations. The Lennard-Jones parameters σ and ϵ are defined in Eq. (16).

T (K)	V (Å^3/atom)	σ (Å)	ϵ (10^{-2} eV)
900	17.370	2.600	4.000
900	18.310	2.600	3.800

A possible source of error might be related to the small system size. In our simulations the periodically repeated supercell contains 64 atoms, whereas Johnson *et al.* have performed MD calculations on a system of 864 atoms. However, if interactions between atoms of different periodic images are included, the use of such a small system causes only a negligible error. Still a cutoff radius $r_{\rm cut}$ needs to be imposed on the LJ interactions, and we took it to be $r_{\rm cut}=8\sigma$ (in all our calculations). We account for the neglect of interactions beyond that distance with the standard correction formulas [that assume $g(r)=1$ for $r>r_{\rm cut}$] that are given by, e.g., Johnson *et al.* [their Eq. (3)] and in Ref. 37. This approach is very satisfactory: Our test at the ($V=18.31$ Å^3, $T=900$ K) thermodynamic state point shows that we can reproduce the potential energy of the fit by Johnson *et al.* to within 1 meV/atom with 64 atoms only. We remark that the inclusion of the LJ interaction between images is entirely consistent with the first-principles treatment of interatomic interactions for which the cutoff distance is practically infinite. Moreover, the good agreement we obtain shows that with 64 atoms and periodic boundary conditions applied the thermodynamic limit can already be closely approached.

2. Calculating the free energy at other thermodynamic state points

Calculation of F for a few thermodynamic state points is not enough: If we want to use Eq. (15) and/or the fit to the simple model to calculate F in their close vicinity, we need to carry out extra simulations (for $\lambda=1$) at those points to obtain the internal energy E and pressure P. The internal energy is obtained straightforwardly as a sum of a kinetic and a potential energy related part:

$$E=\left\langle \sum_i \frac{M}{2}\mathbf{v}_i\cdot\mathbf{v}_i+U(\mathbf{R},T)\right\rangle, \tag{17}$$

where M is the atomic mass and $\mathbf{v}_i$ the velocity of particle i. The brackets denote the thermal average. The pressure is calculated during the MD simulation by means of

$$P=P_{\rm id}(V,T)-\left\langle\frac{dU}{dV}\right\rangle, \tag{18}$$

where the kinetic contribution, $P_{\rm id}$, is the ideal gas pressure. The contribution due to the potential (i.e., arising from $\tilde{F}$) is

obtained via the Hellmann-Feynman theorem. A complication arises due to the incompleteness of the basis set (see Sec. II D).

Knowing F, E, and P at our two reference state points we do not directly proceed by thermodynamic integration of Eq. (15). Instead, inspired by Ref. 11, we introduce a general and physically transparent simple model (all quantities are per atom):

$$F=-3k_{\mathrm{B}}T\,\ln[T/\eta(V)]+E_0(V)+O[(T-T_0)^2], \quad (19)$$

$$S=-\left(\frac{\partial F}{\partial T}\right)_{N,V}=3k_{\mathrm{B}}(\ln[T/\eta(V)]+1)+O(T-T_0), \quad (20)$$

$$E=F+TS=3k_{\mathrm{B}}T+E_0(V)+O(T-T_0). \quad (21)$$

This model constitutes one of various possible, general ways to expand F around the reference temperature T_0 (See Ref. 38). It should be borne in mind that the model parameters (η, E_0), as well as the errors, are volume dependent.

The essential idea behind the model, reflected by the $-3k_{\mathrm{B}}\ln(T)$ contribution to F, is to account for the temperature dependence of the ''harmonic'' contribution to the free energy exactly. (This results in a zero-order approximation of the specific heat c_{V} by its harmonic value $3k_{\mathrm{B}}$.) This gives good hope that the errors are negligible in the (V,T) range of interest.

From now on we neglect the $O(T-T_0)$ and $O[(T-T_0)^2]$ contributions in Eqs. (19), (20), and (21) and use the resulting approximate model to obtain $F(V,T)$ in the vicinity of the two reference points. The strategy is as follows. (a) The model parameters are determined from fits at the reference points. Next the model is used to calculate F and P as a function of T for the two volumes $V_{0,a}$ and $V_{0,b}$. (b) For each temperature, the zero-pressure volume is obtained from a linear interpolation for P between the two volumes. (c) For all temperatures of interest, F at the zero-pressure volume [i.e., $G(P=0)$] is calculated by thermodynamic integration of $P(V)$ [i.e., the first part of Eq. (15)] starting at one of the reference volumes.

The procedure outlined above implicitly assumes a quadratic expansion of $E_0(V)$ with respect to V and a linear expansion of $\ln[\eta(V)]$ with respect to V. This means that five parameters need to be determined, whereas we have six pieces of information available (F, E, and P for the two volumes at $T=T_0$). Therefore we are allowed to do one check on consistency of the model as will become clear at the end of following discussion of steps (a)–(c).

In step (a) we use the second part of Eq. (15) in the context of the approximate model, giving

$$\left(\frac{\partial F}{\partial T}\right)_V=\frac{F-E}{T}=-S=-3k_{\mathrm{B}}(\ln[T/\eta(V)]+1). \quad (22)$$

Substituting our values of F and E at the reference points gives η for both reference volumes. As a next step E_0 can be obtained from substitution of η and the reference point values into Eq. (19) so that F is known as a function of T for both reference volumes. The pressure as a function of temperature can be obtained by integration of

TABLE II. Total energy differences between different crystal structures of Al at their equilibrium volumes. The energies were calculated with different plane-wave cutoff energies E_{cut}.

E_{cut} (eV)	130	170
$E_{\mathrm{hcp}}-E_{\mathrm{fcc}}$ (eV/atom)	0.0305	0.0296
$E_{\mathrm{bcc}}-E_{\mathrm{fcc}}$ (eV/atom)	0.0957	0.0935
$E_{\mathrm{sc}}-E_{\mathrm{fcc}}$ (eV/atom)	0.3719	0.3801

$$\left(\frac{\partial P}{\partial T}\right)_V=-\frac{\partial^2 F}{\partial T\partial V}=-3k_{\mathrm{B}}\frac{d\,\ln\,\eta(V)}{d\,V}, \quad (23)$$

which follows directly from Eq. (22). The need to calculate $d\,\ln(\eta)/d\,V$ explains why F and E have to be calculated for *two* volumes at least. Now both F and P are known as functions of temperature (near T_0) for the two reference volumes.

In step (b) we find the zero-pressure volume (as a function of T) by assuming a linear volume dependence for the pressure.

At step (c) integration of the first expression of Eq. (15) will result in F at the zero-pressure volume, i.e., $G(T,P=0)$.

Note that since we carried out calculations at two reference volumes, we can integrate to the zero-pressure volume in two ways. This provides a good check for consistency and validity of the quadratic form of $E_0(V)$. Moreover, we checked the validity of the neglect of the $O[(T-T_0)^2]$ term in Eq. (19) with test calculations using a restricted **k**-point sampling (at Γ only, see Sec. III A 1 for more details).

D. Technical details

The orbitals and charge density are expanded in plane waves. An ultrasoft pseudopotential (US-PP) of Vanderbilt type[17,18] is used to represent the interaction between valence electrons and the frozen core. [In Eqs. (3) and (4) the extra terms arising from the use of a US-PP have been left out for simplicity.] The plane-wave kinetic-energy cutoff needs to be chosen sufficiently large, i.e., the total-energy difference between various (close-packed) phases should be reasonably well converged. Table II shows results of test calculations on the total energies of the fcc, hcp, bcc, and sc crystals. It follows that the fcc-hcp difference is already well described with a cutoff of 130 eV. With this cutoff the bcc-hcp energy difference is also converged to within 2 meV. For hcp-sc the discrepancies are larger. But this is of little relevance, since the sc structure is very dissimilar to the close packed structures of both the solid and the liquid. In view of these test results, we carried out all calculations with a cutoff of 130 eV. In addition the real-space projection scheme of Ref. 39 was used to efficiently handle the nonlocal part of the electron-ion interaction.

A point of major concern is the convergence of the MD simulations with respect to **k**-point sampling, for both the liquid and the solid. In order to obtain total energies with an accuracy in the meV/atom range, the **k**-point mesh needs to be sufficiently dense. In fact, for Al we would like to use a $4\times4\times4$ Monkhorst-Pack[40] mesh in the BZs of our 32- and 64-atom supercells. However, since the point-group symmetry of our cubic supercell is broken by disorder, this would,

TABLE III. **k** points (in units of the reciprocal lattice vectors) and their weights used for the liquid-state simulations and the calculation of anharmonic effects in the crystal.

k points	Weight
(0.125, 0.125, 0.125)	0.125
(0.375, 0.125, 0.125)	0.375
(0.375, 0.375, 0.125)	0.375
(0.375, 0.375, 0.375)	0.125

in principle, result in the need to calculate the wave functions at all 32 **k** points of equal weight in the BZ. This would render the MD calculation computationally too demanding. Therefore we run our calculations with only the four special points in the irreducible wedge of the cubic BZ, i.e., as if full point-group symmetry still applied. The size of the error incurred by this additional approximation is discussed in Sec. III. The **k** points and their weights are listed in Table III.

Although there is no strict formal justification for the approximation of sampling the wave functions only at the special points, there is a good reason to expect that it will work. It is well known that for simple metals the dominant part of the electronic Hamiltonian is the kinetic energy. This results in a shell-like structure of the electronic density of states with peaks around $\hbar^2/(2m_e)(\mathbf{G}+\mathbf{k})^2$, where **G** represents a reciprocal lattice vector and **k** denotes a vector of the Monkhorst-Pack mesh in the BZ. The kinetic energy is most sensitive to the **k**-point sampling. However, since $(\mathbf{G}+\mathbf{k})^2$ remains invariant under point-group operations, even if the symmetry is broken, the energy is expected to be well approximated with the special points only.

In principle, it is possible to obtain an estimate of the error in F caused by using only the special points (denoted by ''spec'') from

$$F_{\text{full}}-F_{\text{spec}}=-k_{\text{B}}T\,\ln\langle e^{-\beta(\widetilde{F}_{\text{full}}-\widetilde{F}_{\text{spec}})}\rangle, \tag{24}$$

where the brackets denote averaging over the special points ensemble, and ''full'' stands for a sampling throughout the full BZ. It is well known that this approach is problematic: The exponent significantly amplifies the contributions due to those rare events where $\widetilde{F}_{\text{full}}-\widetilde{F}_{\text{spec}}$ is large. In view of this difficulty, one might hope that the errors in the liquid and solid state would cancel, so that there is no need to calculate them. However, at different sides of the phase boundary different parts of phase space are visited and therefore such a cancellation is not guaranteed to occur (even if the liquid and solid systems are of comparable size).

In Eq. (18) the pressure is calculated as the derivative of the potential energy ($\widetilde{F}$) with respect to volume for a fixed basis set. However, our calculations (for several volumes) have been carried out at a constant kinetic-energy cutoff of 130 eV, resulting in a volume-dependent basis set. Therefore, in order to achieve overall consistency, a correction that accounts for the change of the basis set with volume needs to be applied.[41] This is easily done, since the ''constant cutoff'' pressure differs from the ''constant basis set'' pressure by a configuration and nearly *volume*-independent shift of 5–6 kbar.

The equations of motion were integrated with the Verlet algorithm, using a time step of 3 fs. For the liquid-state simulations the temperature was controlled with a Nosé thermostat.[29] For the solid-state simulations an Andersen thermostat was used.[31]

Calculations were carried out using the Vienna *ab initio* simulation package (VASP).[42–44] Details on the minimization techniques employed can be found in Ref. 44. In our liquid-state MD's convergence of $\widetilde{F}$ to 1.5×10^{-6} eV/atom was typically reached in four iterations. In the crystalline state MD's 5–6 iterations were needed to attain the specified tolerance of 1.5×10^{-6} eV/atom. A slightly worse convergence is to be expected since the random noise introduced by the Andersen thermostat partly frustrates the construction of a good initial guess for the charge density and wave functions extrapolated from previous MD steps.

III. APPLICATION TO THE MELTING OF Al

In the following we apply the methods described in the previous section to the calculation of the melting transition of aluminum. First (Sec. III A) we discuss the errors for both the liquid and solid state separately. Then results for the melting properties are presented (Sec. III B).

A. Error estimation

1. Liquid state

The errors can be subdivided into two distinct classes. First, there are those that arise from inaccuracies in the treatment of the electronic structure part of the calculation. Second, there are those that originate from the various approximations needed to calculate the thermodynamic potentials from the interatomic interactions.

The main error from the first class is that due to the reduced **k**-point sampling (See Sec. II D). Before starting our first-principles MD simulations we carried out a test on a set of configurations obtained from an MD using a Al pair potential from second-order perturbation theory. For these configurations we calculated the electronic free energy $\widetilde{F}$ for various **k**-point meshes. We took the $4\times4\times4$ Monkhorst-Pack mesh as a reference (i.e., 32 **k** points in the BZ). We found that, for Γ-point sampling only, $\widetilde{F}$ was underestimated by ~0.02 eV/atom. With a $2\times2\times2$ Monkhorst-Pack mesh it was overestimated by the same amount. When using only those four **k** points of the $4\times4\times4$ mesh that are in the irreducible wedge of the cubic BZ (assuming full cubic symmetry, see Table III), the maximum error was reduced to ~2 meV/atom and the average error was a mere ~0.4 meV/atom. This motivated us to use these four special points in the first-principles simulations. However, since these tests were carried out on configurations obtained from a sampling of phase space using only a pair potential, the test results do not provide more than an indication. Therefore, we carried out convergence tests during first-principles MD simulation also, and the results are listed in Table IV. It can be seen that differences as large as 2.5 meV occur when using the full $4\times4\times4$ mesh instead of our 4 special points. Differences with respect to calculations using a denser **k**-point mesh $(6\times6\times6)$, but using also only those points that

TABLE IV. Convergence tests of $\tilde{F}$ with respect to the **k**-point mesh for several configurations sampled at 0.225-ps intervals along the trajectory of the liquid-state first-principles MD run $V=17.37$ Å^3, $T=900$ K. $\tilde{F}$ is in meV/atom and measured relative to the $\tilde{F}$ from the first-principles MD run (i.e., ''4×4×4, IRR''). The Monkhorst-Pack mesh is indicated and IRR indicates that only the irreducible part of the high-symmetry cubic zone has been used.

	IRR 4×4×4	4×4×4	IRR 6×6×6
	0	0.0	1.8
	0	−0.4	−0.3
	0	1.8	0.4
	0.	1.5	1.1
	0	0.0	1.1
	0	2.3	0.2
	0	1.3	1.5
	0	2.5	0.3
	0	−1.7	0.5
	0	1.5	0.0
	0	−0.1	0.8
	0	1.9	0.6
	0	−0.4	−0.6
	0	−0.6	1.0
	0	−0.7	0.6
	0	−0.2	0.4
Averages:		0.5	0.6

are in the irreducible wedge of the cubic BZ, are smaller.

The errors of the second class can themselves be subdivided into errors of two kinds. First, there are the errors caused by our limited *statistical* sampling, that propagate into the calculation of G. Second, there are the *systematic* errors caused by the approximations made to fit the model and do the thermodynamic integrations. These two kinds of errors are discussed in the rest of this section.

Discussion of the statistical errors is most straightforward. The free energies, internal energies and pressures, for the reference states $(T_0,V_{0,a})$ and $(T_0,V_{0,b})$, along with their estimated errors are summarized in Table V. The production runs were too short (ranging from 1.5 to 1.9 ps) to allow for a thorough statistical analysis that could give a good estimate of the standard deviations of the mean values.[37] Instead we give estimates based on comparisons of variable length running averages.

A remark is in order on how the free energies in Table V were calculated. The coupling constant integrations were carried out using only one ensemble ($\lambda=0.5$) to approximate the integral of Eq. (7). As can be seen from, e.g., Fig. 1 the LJ system can be tuned to approach the first-principles system very closely (See Table I for details). Nevertheless, it is not guaranteed that the integral is well approximated by the halfway point only. (Moreover, some difference had to be allowed for in order to keep the LJ system out of the nonliquid region of its phase diagram.) We assessed the validity of this approximation with a test calculation where we used a sampling of the wave functions at Γ only (instead of sampling at the four special points). Since this reduces the computational demand by nearly a factor 8, this test is not prohibitively expensive and we can run three ensembles ($\lambda=\{0,0.5,1\}$) instead of just one. It is found that the result of a Simpson integration using all three ensembles differs from the result obtained with $\lambda=0.5$ by less than 1 meV/atom.

TABLE V. Calculated thermodynamic data for the liquid at the reference points ($T=T_0$, $V=\{V_{0,a},V_{0,b}\}$) and their estimated statistical errors (in parenthesis) for the liquid state.

T (K)	900	900
V (Å^3/atom)	17.370	18.310
F (eV/atom)	−4.4524 (0.001)	−4.4608 (0.001)
E (eV/atom)	−3.841 (0.002)	−3.818 (0.002)
P (kbar)	25 (2)	0 (2)

Having obtained F, E, and P at the reference points, we next need to carry out step (a) of Sec. II C 2. However, before doing so, we first need to assess the validity of the neglect of the $O[(T-T_0)^2]$ term in Eq. (19). We again use the computationally convenient test system with sampling at Γ only. For $V=18.31$ Å we calculate η and E_0 from F and E at $T=900$ K. Next we use Eq. (19), discarding the correction term, to calculate the Helmholtz free energy at $T=750$ K and compare it to the value obtained directly from coupling constant integration. Agreement is found to be much better than the ~ 1 meV/atom error bar. This shows that the temperature dependence of F is well described neglecting the $O[(T-T_0)^2]$ term. Using Eq. (22) it easily follows how the errors grow while integration along T proceeds:

$$\sigma(F(T))=\sigma(F_0)+\frac{T-T_0}{T_0}(\sigma(F_0)+\sigma(E_0)), \qquad (25)$$

where the σ's are the standard deviations. This formula shows that the distance of T from T_0 needs to be considerable before serious deterioration of the error occurs, provided that $\sigma(E_0)$ is not significantly larger than $\sigma(F_0)$.

To complete the first stage (a) we also integrate Eq. (23) along T to obtain $P(T)$ at both reference volumes. Generally this results in an error in P of ~ 1 kbar for a change of ~ 100 K.

In the next stage (b) we calculate the zero-pressure volume from a linear interpolation of P between $V_{0,a}$ and $V_{0,b}$. Here, as well as in the following, we need to apply the correction to P so as to make it consistent with our constant cutoff calculations (See Sec. II D).

At the last stage (c) we integrate the first equation of Eq. (15) along V from the reference volume (note that here we have two possibilities) to the zero-pressure volume and obtain $F=G(P=0)$ at this volume. Of course several assumptions enter into this procedure that do not seem immediately justified *a priori*, such as the linear dependence of P on volume. However, fortunately a check on the correctness of these assumptions exists in the comparison of the two values obtained from integration starting from the two different reference points.[45] Here we find that the values obtained by the two routes differ by about 1 meV/atom, showing that our assumptions were indeed justified.

2. Solid state

Following the methodology described in Sec. II B the PDOS and the equilibrium energy $U_0(V,T)$ are calculated at a set of volumes ($V/\text{Å}^3/\text{atom}=\{14.82,16.30,17.78,19.26\}$). From this the Helmholtz free energy F is obtained using Eq. (9). For every temperature of interest, the volume dependence is fitted by a polynomial and the Gibbs free energy, in the quasiharmonic approximation, is obtained through Eq. (5).

We already noted that the error caused by ignoring the temperature dependence of the PDOS is negligible (Sec. II B 1). Moreover, such an error does not occur for U_0 since its temperature dependence is fully accounted for.

The neglect of part of the force constants matrix caused by the finite size of the supercell also gives rise to an error in the PDOS. To have a check on the size of this error we carried out calculations for 32- and 108-atom supercells, with Monkhorst-Pack meshes of $6\times6\times6$ and $4\times4\times4$, respectively. This gives the same **k**-point density for both cells. The effect on G was found to be very small: For the larger supercell G is approximately 0.5 meV/atom lower (in the 800–1000 K temperature range). Therefore this error can also be considered negligible. We expect that the results are converged with respect to the **k**-point sampling, since in test calculations ($V=17.78$ Å^3) use of the $4\times4\times4$ instead of the $6\times6\times6$ mesh for the 32-atom cell results in a change of F of 1 meV/atom only.

The corrections for anharmonicity are applied using the coupling constant integration technique. For one temperature ($T=850$ K) the corrected Helmholtz free energy is calculated at three volumes. It is extrapolated to other volumes *via* a fit to a polynomial. The temperature dependence is obtained assuming a T^2 scaling. This is checked by one calculation of the anharmonic correction at $T=1000$ K, and found to be correct within the statistical error bar. However, scaling linear with T would also fit within the accuracy. Since our calculated melting temperature is found to be 890 K (see below), i.e., very close to 850 K, the exact nature of the scaling is irrelevant because it induces a negligible error. The anharmonic corrections to F obtained in this way are added to the harmonic part of F and G is obtained from Eq. (5) as usual.

In contrast to the harmonic free energy, which was not obtained from simulation but which was directly calculated, the coupling constant integration is subject to statistical errors. These are reasonably well under control and ~1 meV/atom (runs were of 1.5–2.7 ps duration and each atomic velocity component was randomly drawn from a Gaussian distribution on average every 0.06 ps). Due to the computational demand of the simulations, more important systematic errors cannot be avoided. In particular, we run with a supercell containing 32 atoms only, and we are forced to restrict our BZ sampling severely. We use the same **k**-point mesh as in our liquid-state MD's, i.e., the four special points of the $4\times4\times4$ Monkhorst-Pack mesh in the BZ of the cubic supercell (Table III). Table VI shows how well the total electronic free-energy correction (i.e., $\widetilde{F}-\widetilde{F}_{\text{HA}}$ where $\widetilde{F}_{\text{HA}}$ is calculated directly from the interatomic force constants matrix $\mathbf{D}_V$) is converged with this mesh compared to other **k**-point meshes, for a few configurations along our $\lambda=0.5$ and $\lambda=1.0$ trajectories at 1000 K. It can be seen that the error is of the order of 3 meV/atom.

TABLE VI. Convergence tests of $\widetilde{F}-\widetilde{F}_{\text{HA}}$ (i.e., the difference between $\widetilde{F}$ calculated entirely from the Mermin functional and $\widetilde{F}_{\text{HA}}$ as obtained from in the quasiharmonic approximation *via* the force constants matrix) with respect to the **k**-point mesh for several configurations along the $\lambda=0.5$ and $\lambda=1.0$ (i.e., fully first-principles) trajectories at $T=1000$ K, $V=17.57$ Å^3. $\widetilde{F}$ is in meV/atom. Both $\widetilde{F}$ and, *via* the interatomic force constants matrix, $\widetilde{F}_{\text{HA}}$ have been calculated using the same **k**-point mesh. The Monkhorst-Pack mesh is indicated and IRR denotes that only the irreducible part of the high-symmetry cubic zone has been used.

	IRR $4\times4\times4$	$4\times4\times4$	IRR $6\times6\times6$
		$\lambda=0.5$	
	6.0	4.1	5.6
	23.9	20.8	21.2
	14.9	12.0	13.0
	13.4	10.1	11.3
	14.3	13.9	13.8
Averages:	14.5	12.2	13.0
		$\lambda=1.0$	
	3.0	5.9	4.2
	6.3	5.7	6.2
	−6.8	−3.5	−4.2
	5.6	9.0	10.0
	2.2	4.3	6.3
	−12.2	−8.5	−7.7
	2.3	5.3	4.1
	−0.3	−0.1	−0.5
	8.3	3.7	7.2
	7.1	4.2	5.3
Averages:	1.6	2.6	3.1

Coupling constant integration was found not to be very well converged using the halfway MD (i.e., $\lambda=0.5$) only. Therefore integrations were done using Simpson's rule from the runs with $\lambda=\{0,0.5,1\}$.

The corrections for anharmonicity are not negligible. They significantly destabilize the solid, in that they raise G by an amount of the order of 10 meV resulting in a reduction of the melting temperature from ~970 K to 890 K.

B. Results

Figure 2 shows the liquid- and solid-state Gibbs free energies near the melting transition at zero pressure. Error bars accounting for the estimated *statistical* errors are included. This does not include the error made due to the limited **k**-point sampling.

The calculated melting properties are compared with experimental data in Table VII (again only the *statistical* errors are included). In general, agreement with experiment is good. The melting transition is found to occur at $T=890\pm20$ K, compared with the experimental value of

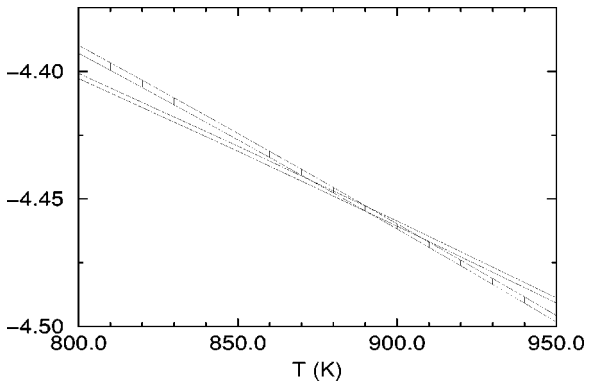

FIG. 2. Calculated Gibbs free energies for the solid and liquid state at zero pressure. The width of the lines represents the statistical error.

933 K. The entropy of fusion s_m is calculated from the slopes of the curves in Fig. 2 using Eq. (1). ΔE, the change in internal energy at melting, than simply follows from $\Delta E = T_m s_m$. The volume change at melting, ΔV, is trivially obtained as the difference between the zero-pressure liquid and crystalline phase volumes (at the calculated melting temperature). Unfortunately, the error bar on the volume discontinuity at melting is rather large. This is mainly due to uncertainties in the anharmonic corrections in the solid state.

The change of the melting temperature with external pressure can be obtained in two ways. From the Clapeyron equation one easily obtains

$$\frac{dP}{dT_m} = \frac{s_m}{\Delta V}, \tag{26}$$

which relates dP/dT_m to known quantities. Alternatively, the whole procedure of Sec. II can be repeated for arbitrary external pressures by just changing the value of P in Eq. (5). Of course, this is only possible as long as we remain close to our reference state points. The existence of these two routes provides a check on the internal consistency of our fitting approach.

TABLE VII. Comparison between experimental and calculated melting related properties of Al. All calculated properties (including estimated statistical errors) are obtained for the calculated melting temperature at zero pressure. Listed are the melting temperature (T_m), the entropy of fusion s_m, the change in internal energy upon melting ΔE (simply related to s_m by $\Delta E = T_m s_m$), the change of volume upon melting ΔV, and the derivative of the melting T_m with respect to pressure.

	Experiment	Calculation
T_m (K)	933.47[a]	890 ± 20
s_m (k_B)	1.38[b]	1.36 ± 0.04
ΔE (mRy)	8.16[b]	7.7 ± 0.2
ΔV (Å^3)	1.24[c]	1.26 ± 0.2
ΔV (Å^3)	0.96[d]	1.26 ± 0.2
dT_m/dP (K/GPa)	65[e]	67 ± 12[f]
dT_m/dP (K/GPa)	65[e]	62[g]

[a] *CRC Handbook of Chemistry and Physics*, 74th ed., edited by D. R. Lide (CRC, Boca Raton, 1994).

[b] Ref. 7.

[c] From the Clapeyron equation, using $\Delta E = 8.16$ mRy and $dT_m/dP = 65$ (K/GPa) at 933 K.

[d] S. P. Kazachkov, N. M. Kochegura, and E. A. Markovskiy, Russ. Metall. **1/1979**, 65 (1979).

[e] J. F. Cannon, J. Phys. Chem. Ref. Data **3**, 781 (1974).

[f] From the Clapeyron equation, using calculated ΔE and ΔV at 890 K.

[g] Directly calculated, i.e., from the change of the melting temperature with pressure.

IV. DISCUSSION & CONCLUSIONS

In this paper we have demonstrated that the melting properties of a metallic element can be calculated with satisfactory accuracy entirely from first principles. In contrast to previous calculations on the melting of metals, the thermodynamic quantities that we have calculated for solid and liquid Al refer to fully first-principles representations of the system, i.e., neither to models fitted to first-principles calculations nor to effective interactions based on a perturbation expansion. This is a crucial methodological distinction, because fitting and/or perturbational procedures may (in principle) introduce completely uncontrollable errors. Such errors are not expected to occur for a simple *sp* bonded metal at ambient pressure, like, e.g., the Al system studied here.[8–11] However, we expect that in cases where a perturbational approach breaks down and/or approximations remain debatable, the present calculational framework can be very helpful. With the present study on a ''test case'' like liquid Al we hope to have demonstrated its feasibility, and pointed out where possible ''bottlenecks'' are to be expected.

It is because we are concerned with general methods that we have placed such a strong emphasis on technicalities, and particularly on the precision of the calculations. We have pointed out that the precision required of the calculated free energies is governed by the entropy of fusion, and for Al this implies that the free energies of the solid and liquid must both be calculated to a precision of a few meV/atom in order to obtain meaningful melting properties. Here, we must distinguish sharply between two completely different questions. The first is the accuracy of DFT (or rather LDA) itself, i.e., its ability to reproduce melting properties given that it is implemented with no imprecision whatever. The second is the technical precision with which DFT has been implemented in the context of fully first-principles calculations. Although we have not been primarily concerned with the inherent accuracy of DFT, we do expect it to be very good for Al.[11] This is not because DFT gives the total energy of Al to an accuracy of a few meV/atom (it clearly doesn't), but because solid and liquid Al are both nearly-free-electron metals, so that there should be an extremely effective cancellation of DFT errors between the two phases. This is why our good agreement with experiment can be taken as confirming the technical quality of the methods we have used. However, we stress again that our main concern has not been with the accuracy of DFT, but with the technical precision of the calculations within DFT.

The question of precision is crucial because the whole approach depends on *independent* calculations of the solid and liquid free energies, and many of the technical errors

cannot be expected to cancel between the two. This is why we must achieve a precision of a few meV/atom for each free energy separately. There are many kinds of technical errors, and we have made a determined effort to reduce them all below the required tolerance. We can broadly divide the errors into statistical and nonstatistical. We have shown that the statistical errors, associated with the limited sampling of phase space in the MD simulations, can be reduced below the tolerance with fairly short runs of only a few ps. The main kinds of nonstatistical errors are (i) errors of thermodynamic interpolation and extrapolation, such as the use of the model of Sec. II C 2 to obtain the liquid free energy at volumes and temperatures other than those explicitly calculated; (ii) errors in thermodynamic integration arising from the use of only a few λ values; (iii) errors due to finite system sizes; (iv) errors due to incompleteness of the plane-wave basis; and (v) **k**-point sampling errors. We have provided detailed evidence to show that the errors (i)–(iv) can be brought under control. We have also done extensive tests that suggest that for Al the **k**-point errors have also been reduced to the required size for both solid and liquid. Nevertheless, we are not completely satisfied, because we have had to economize by sampling only over the irreducible zone (of the high-symmetry fcc cell) at certain points in the calculations. The evidence we presented indicates that this is satisfactory for a nearly-free-electron metal like Al. But this means that we are losing generality, and we believe there is a need for further work on the **k**-point problem.

We conclude by commenting on the pioneering first-principles work of Sugino and Car on the melting of Si.[3] We note that our agreement with experiment is somewhat better than theirs, since our calculated T_m differs from the true value by less than 5%, whereas theirs was off by $\sim 20\%$. However, one should not draw hasty conclusions. It is very likely that the inherent accuracy of the LDA is worse for the melting of Si than for that of Al, since Si is a semiconductor on one side of the transition and a metal on the other, whereas Al is a metal on both sides. This means that electronic screening, and the nature of the exchange-correlation hole will change when Si melts, and this change may not be well described by LDA. For Al, the cancellation of LDA errors should be better. On the other hand, the problems of technical precision look worse for Al, because its entropy of fusion is less than half of the value in Si (1.38 k_B rather than 3 k_B), and its melting temperature is only half the size (933 rather than 1685 K). This means that the tolerance needed to get a given percentage precision in T_m is about four times smaller in Al. The fact that we have needed to use a **k**-point mesh that is eight times denser than that used by Sugino and Car is no doubt linked with this.

Building on the success of this work, we are now studying the problems of doing similar calculations on more challenging systems, including transition metals.

ACKNOWLEDGMENTS

The work of G.A.d.W. is supported by NERC Grant No. GST/02/1454 and that of G.K. by EPSRC Grant No. GR/L08946. We thank the High Performance Computing Initiative for allocations of time on the Cray T3D at Edinburgh Parallel Computer Center, these allocations being provided through the Minerals Consortium and the U.K. Car-Parrinello Consortium. We also acknowledge an allocation of time on the Cray J90 at the Atlas Laboratory. Discussions with Professor G. D. Price, Dr. L. Vočadlo, Dr. J. Furthmüller, Professor D. Frenkel, and Professor P. A. Madden are gratefully acknowledged.

*Present address: Electronic Structure of Materials, Research Institute of Materials, KUN, Toernooiveld 1, 6525 ED Nijmegen, The Netherlands.

†Present address: Institute for Theoretical Physics, Technical University of Vienna, Wiedner Hauptstraße 8-10/136, A-1040 Vienna, Austria.

[1] R. O. Jones and O. Gunnarsson, Rev. Mod. Phys. **61**, 689 (1989).

[2] R. Car and M. Parrinello, Phys. Rev. Lett. **55**, 2471 (1985).

[3] O. Sugino and R. Car, Phys. Rev. Lett. **74**, 1823 (1995).

[4] E. Smargiassi and P. A. Madden, Phys. Rev. B **51**, 117 (1995).

[5] R. Car, P. E. Blöchl, and E. Smargiassi, Mater. Sci. Forum **83–87**, 443 (1992); E. Smargiassi and R. Car, Phys. Rev. B **53**, 9760 (1996).

[6] V. Milman, M. C. Payne, V. Heine, R. J. Needs, J. S. Lin, and M. H. Lee, Phys. Rev. Lett. **70**, 2928 (1993).

[7] M. W. Chase, Jr., C. A. Davies, J. R. Downey, Jr., D. J. Frurip, R. A. McDonald, and A. N. Syverud, J. Phys. Chem. Ref. Data Suppl. **14**, 1 (1985).

[8] J. A. Moriarty, D. A. Young, and M. Ross, Phys. Rev. B **30**, 578 (1984).

[9] J. L. Pélissier, Physica A **128**, 363 (1984).

[10] J. Mei and J. W. Davenport, Phys. Rev. B **46**, 21 (1992).

[11] G. K. Straub, J. B. Aidun, J. M. Wills, C. R. Sanchez-Castro, and D. C. Wallace, Phys. Rev. B **50**, 5055 (1994).

[12] To avoid confusion, all thermodynamic functions referring to the electronic subsystem have been labeled with a tilde. In those functions the atomic positions enter as a parameter only.

[13] N. D. Mermin, Phys. Rev. **137**, A1441 (1965).

[14] M. J. Gillan, J. Phys.: Condens. Matter **1**, 689 (1989)

[15] D. M. Ceperley and B. J. Alder, Phys. Rev. Lett. **45**, 566 (1980).

[16] J. P. Perdew and A. Zunger, Phys. Rev. B **23**, 5048 (1981).

[17] D. Vanderbilt, Phys. Rev. B **41**, 7892 (1990).

[18] G. Kresse and J. Hafner, J. Phys.: Condens. Matter **6**, 8245 (1994).

[19] S. G. Louie, S. Froyen, and M. L. Cohen, Phys. Rev. B **26**, 1738 (1982)

[20] R. P. Feynman, Phys. Rev. **56**, 340 (1939).

[21] R. M. Wentzcovitch, J. L. Martins, and P. B. Allen, Phys. Rev. B **45**, 11 372 (1992).

[22] M. Weinert and J. W. Davenport, Phys. Rev. B **45**, 13 709 (1992).

[23] D. Frenkel and B. Smit, *Understanding Molecular Simulation* (Academic Press, San Diego, 1996).

[24] J. K. Johnson, J. A. Zollweg, and K. E. Gubbins, Mol. Phys. **78**, 591 (1993).

[25] M. Watanabe and W. P. Reinhardt, Phys. Rev. Lett. **65**, 3301 (1990).

[26] D. C. Wallace, *Thermodynamics of Crystals* (Wiley, New York, 1972).

[27] To avoid confusion, a vector in the Brillouin zone is denoted by **k** if it labels a Kohn-Sham state and denoted by **q** if it labels a phonon.

[28] G. Kresse, J. Furthmüller, and J. Hafner, Europhys. Lett. **32**, 729 (1995).

[29] S. Nosé, J. Chem. Phys. **81**, 511 (1984).
[30] G. J. Martyna, M. L. Klein, and M. Tuckerman, J. Chem. Phys. **97**, 2635 (1992).
[31] H. C. Andersen, J. Chem. Phys. **72**, 2384 (1980).
[32] R. E. Swanson, G. K. Straub, B. L. Holian, and D. C. Wallace, Phys. Rev. B **25**, 7807 (1982).
[33] R. O. Simmons and R. W. Balluffi, Phys. Rev. **117**, 52 (1960).
[34] B. Henderson, *Defects in Crystalline Solids* (Edward Arnold, London, 1972).
[35] J. A. Moriarty, in *Many-Atom Interactions in Solids*, edited by R. M. Nieminen, M. J. Puska, and M. J. Manninen (Springer, Berlin, 1990).
[36] D. B. Boercker and D. A Young, Phys. Rev. A **40**, 6379 (1989).
[37] M. P. Allen and D. J. Tildesley, *Computer Simulation of Liquids* (Clarendon Press, Oxford, 1987).
[38] Note that our formula for $F(V,T)$ is nothing more than a Taylor expansion of this function with respect to T around the reference temperature T_0 out of which the ''harmonic contribution'' ($\sim \ln T$) has been explicitly isolated.
[39] R. D. King-Smith, M. C. Payne, and J. S. Lin, Phys. Rev. B **44**, 13 063 (1991).
[40] H. J. Monkhorst and J. D. Pack, Phys. Rev. B **13**, 5188 (1976).
[41] M. C. Payne, M. P. Teter, D. C. Allan, T. A. Arias, and J. D. Joannopoulos, Rev. Mod. Phys. **64**, 1045 (1992).
[42] G. Kresse and J. Hafner, Phys. Rev. B **47**, 558 (1993); *ibid.* **49**, 14 251 (1994).
[43] G. Kresse and J. Furthmüller, Comput. Mater. Sci. **6**, 15 (1996).
[44] G. Kresse and J. Furthmüller, Phys. Rev. B **54**, 11 169 (1996).
[45] The volume integration can only be done for the system with all four **k** points included. With the increase of volume, stars of plane waves move into the sphere within the cutoff radius giving rise to discontinuous jumps in P. These jumps become less noticeable with the increase of the density of the **k**-points mesh. When sampling at Γ only, the **k**-point mesh is not dense enough and the discontinuities spoil the volume integration.